Journal of Thermal Analysis and Calorimetry (2022) 147:12467–12479
https://doi.org/10.1007/s10973-022-11450-0

Thermal behavior of gamma-irradiated urea–formaldehyde composites based on the differently activated montmorillonite K10

Suzana Samaržija-Jovanović[1] · Vojislav Jovanović[1] · Tijana Jovanović[2] · Branka Petković[1] · Gordana Marković[3] · Slavica Porobić[4] · Milena Marinović-Cincović[4]

Received: 7 October 2021 / Accepted: 9 June 2022 / Published online: 9 July 2022

Abstract
This work investigated the thermal characteristics of irradiated composite materials formulated on the urea–formaldehyde resin (UF) and differently activated montmorillonite (K10). UF resin with molar ratio $F{:}U = 0.8$ was synthesized in situ with differently activated K10. K10 was activated by heating at 400 °C, with sulfuric acid (H_2SO_4) without and with magnetic stirring. The samples are marked with TK10, AK10, ASK10, UF/TK10, UF/AK10, and UF/ASK10, respectively. The samples were identified by applying X-ray diffraction analysis and thermal methods (TGA and DTA), supported by data from Fourier Transform Infrared spectroscopy and scanning electron microscopy. The degree of activation was determined by measuring specific surface area (SSA) using Sear's method. Measurement of the value for SSA shows that the sample TK10 has the highest value (317 $m^2\ g^{-1}$) among the other two samples, (for AK10 = 183 $m^2\ g^{-1}$ and ASK10 = 167 $m^2\ g^{-1}$). The modified UF/AK10 composite is more thermally stable than other two modified UF/K10 composites.

Keywords γ-Irradiation · Montmorillonite · UF resin · Thermal stability

Introduction

Urea–formaldehyde (UF) resins, a polymer product of the condensation of urea and formaldehyde, are one of the most important adhesives. They are thermosetting resins consisting of oligomeric and polymeric molecules, which always contain a certain amount of monomers. Unreacted urea is often useful, especially because of the better stability during storage. However, the presence of free formaldehyde is ambivalent [1–3]. UF resins and its products are widely used in wood industry due to superior characteristic, such as colorlessness, fast curing, water solubility, and low cost [4–6]. In addition, they are characterized by excellent electrical and thermal insulation properties, a wide range of toughness, elasticity, and resistance to solvents and chemicals. However, UF resins also have several disadvantages, such as low water resistance and formaldehyde emissions from UF adhesive bonded panels. These disadvantages somewhat limit their use as adhesives for wood panels for interior use [7].

Composites obtained by the synthesis of organic polymers and inorganic clay materials such as montmorillonite (MMT) containing aluminosilicate layers, cause great attention due to improved mechanical and better thermal properties but without a significant increase in density that cannot be achieved with conventional fillers [8–10]. Layered silicates commonly used in the preparation of polymeric layered silicate composites belong to the general 2:1 family of phyllosilicates. MMT is one of the hydrated aluminosilicates type 2:1 with an octahedral sheet inserted between two tetrahedral plates. Replacement of cations at tetrahedral and mainly at octahedral sites gives a negative layer charge of about 0.2–0.5 eV. The layered charge is compensated by the introduction of interchangeable interlayer cations (Na^+, Ca^{2+}, Mg^{2+}, etc.). They are usually in hydrated form, which in turn provides adsorption sites on the inner and outer

✉ Suzana Samaržija-Jovanović
vojani@sbb.rs; suzana.samarzija@pr.ac.rs

1 Faculty of Sciences and Mathematics, University of Priština in Kosovska Mitrovica, Lole Ribara 29, 38220 Kosovska Mitrovica, Serbia

2 Faculty of Sciences and Mathematics, University of Niš, Višegradska 33, 18000 Niš, Serbia

3 A.D. Tigar, Nikole Pašića 213, 18300 Pirot, Serbia

4 Vinča Institute of Nuclear Sciences - National Institute of the Republic of Serbia, University of Belgrade, Mike Petrovića Alasa 12-14, 11000 Belgrade, Serbia

surface of the crystal. These characteristics of the structure of montmorillonite determine the specific properties of bentonite clays, especially the high adsorption capacity [11–14]. MMT has exceptional physicochemical characteristics such as high specific surface area (SSA), strong adsorption affinity, low permeability, high cation exchange capacity, high swelling properties, stability, and low cost [15].

Modification of MMT can affect its structural properties such as the chemical composition of the clay, interchangeable cations in the interlayer, textural properties such as SSA, porosity, or acidic properties [16]. Some of the methods used to modify MMT are acid activation, thermal activation or calcination, pillaring, activation by ultrasonic waves, etc.

In the process of thermal calcination, which is an effective way to activate MMT, four reactions occur (1) dehydration, (2) dehydroxylation, (3) decomposition, and (4) recrystallization. Water in the interlayers is lost at temperatures higher than 220 °C, and dehydroxylation takes place in the temperature range of 350–1000 °C [15].

The method of acid activation of clays is used to modify different types of clays with the aim of improving their physicochemical properties in order to expand the field of their application in the industry. Acid-activated clays are most often used in industry as adsorbents, bleaches, and catalysts [17]. From the point of view of industrial application of clay, the term "acid-activated clays" refers mainly to acid-activated bentonite due to their large application in various industries. For example, treatment of Ca^{2+}-bentonite with inorganic acids increases its specific surface area and porosity due to disruption of smectite structure (basic bentonite builders) caused by the exchange of Ca^{2+} from octahedral layers with H^+, OH^- ion binding, and formation of amorphous silicate phase [18].

One of the common methods used to modify polymeric materials is the gamma ray irradiation method (γ-irradiation). By exposing polymeric materials to gamma rays, reactive intermediates (free radicals, ions, and excited states) are created. The degree of modification of polymers depends on the type of polymeric material and irradiation conditions. Polymers exposed to gamma rays are subject to the process of crosslinking and degradation. Which of these two processes will be dominant depends on the structure of the polymer material [19].

In this paper, the structure of differently activated K10 as well as the thermal stability of modified γ-radiated UF/K10 composites were investigated.

Experimental

Urea (produced by Alkaloid-Skopje, North Macedonia); 35% Formaldehyde (produced by Unis-Goražde, Bosnia and Herzegovina); Montmorillonite-K10 (produced by Sigma-Aldrich Chemistry, Germany) with SSA of 220–270 $m^2\ g^{-1}$ were used. All the chemicals and solvents used in the experimental part were of analytical quality.

Modification of montmorillonite K10

Method thermal activation of montmorillonite

In order to obtain samples of modified montmorillonite, thermal activation of montmorillonite K10 was performed according to the literature [20].

Acid activation of montmorillonite

Another method of modification of montmorillonite K10 was by acid activation known in the literature [20].

Activation of montmorillonite by stirring on a magnetic stirrer

The activation of montmorillonite was performed by dispersing 5 g of acid-activated montmorillonite in 100 mL of distilled water following [21]. The reaction mixture was stirred on a magnetic stirrer for 15 min at a rate of 550 rpm min^{-1}. The suspension was allowed to settle, after which the liquid was decanted. The montmorillonite was then dried at 105 °C for 6 h or constant mass.

Synthesis and irradiation of UF/K10 composites

A two-step alkaline-acid process was used to synthesize modified UF/K10 composites with molar ratio of UF/U = 0.8 [22]. γ-Irradiation of UF/K10 composites were performed in the Co-60 radiation unit at the Vinča Institute of Nuclear Sciences—National Institute of the Republic of Serbia. Data on the Radiation Unit are described in the literature [23]. The samples UF/K10 were irradiated in air with the dose rate about 10 kGy h^{-1} and total absorbed dose of 50 kGy.

Characterization of the K10, modified K10 and synthesized modified UF/K10 composites

The SSA of MMT was determined using the Sear's method [24]. The volume (V) required to raise the pH from 4 to 9 is recorded and the SSA was calculated by Eq. (1):

$$\text{SSA}\ (m^2\ g^{-1}) = 32 \cdot V - 25. \quad (1)$$

Micrographs of the activated and pure K10 were taken with a Tescan FE-SEM Mira 3 XMU scanning electron microscope at 20 kV acceleration voltage. Prior to recording, the samples were steamed with gold on a Polaron SC503, Fisons Instruments.

Device Rigaku (Japan) SmartLab diffractometer was used for XRD measurements. Measurements were performed in a 2θ range from 10° to 80° counting 10° min^{-1} in 0.02° steps. The percentage of crystallinity of modified K10 and synthesized modified UF/K10 composites was calculated by Eq. (2) from the XRD patterns using the peak deconvolution method with a Gaussian function [25]:

$$\text{Crystalinity } (\%) = \frac{\text{area of crystalline peaks}}{\text{area of all peaks}} \cdot 100. \quad (2)$$

The crystallite size-D (nm) was estimated using the Scherrer equation Eq. (3):

$$D = \frac{k \cdot \lambda}{\beta \cdot \cos \Theta}, \quad (3)$$

where k is a constant factor ($k = 0.9$), λ is the wavelength of the X-ray radiation ($\lambda = 0.15406$ nm), β is the width at half maximum intensity in radians (FWHM), and θ is Bragg's angle in radians (peak position).

FTIR spectra of samples were recorded at room temperature in the wavenumber range of 4000–500 cm^{-1} on a Nicolet spectrophotometer (Model 380, Thermo Nicolet Corporation, Madison, USA).

Thermal characteristics of composite samples were performed by the usual method of non-isothermal thermogravimetry (TG, DTA) on the device Setaram Setsis Evolution 1750. The test samples were heated in the range from 30 to 800 °C with a heating rate of 10 °C min^{-1} and a gas flow of 20 cm^3 min^{-1}, in the argon atmosphere.

Results and discussion

The properties of the polymer-filler mixture depend on the characteristics of the filler (shape and size) and the properties of the polymer matrix (molecular weight, structure, compatibility with particles). Filler and polymer play an important role in modeling the properties of UF composites. The added filler increases the volume, reduces the product's price, and significantly affects properties such as the content of free and released formaldehyde in the UF resin. The key component or functional material of these composites is reinforcing nanofillers, and by designing and optimizing mixtures with different combinations of these fillers, the properties of the obtained composites can be designed and optimized. In this way, mechanical properties are improved, such as the hardness and strength of products based on UF resins, and thermal properties, especially if we keep in mind that the gluing of plywood panels takes place at high temperature and pressure. Today, research goes in the direction of interactions between filler surface and polymer molecules, but other factors such as the influence of filler surface chemistry, morphology, and specific interactions between filler particles and polymer macromolecules must be taken into account [26].

The chemical composition, the nature of surface atoms (mainly hydrogen and oxygen), the existence and type of defective sites, the charge of layers, and the type of exchangeable cations are just some of the factors that affect the surface properties of clay minerals [18].

Figure 1 shows a graphical representation of the dependence of SSA on the modification method K10 determined by Sear's method. The SSA of unmodified montmorillonite K10 was 119 m^2 g^{-1} as it has been shown by Samaržija-Jovanović et al. [27]. After using different modification (activation) methods, the specific surface area was 183 m^2 g^{-1} for the sample activated with acid (AK10), 167 m^2 g^{-1} for the sample additionally activated by mixing on a magnetic stirrer (ASK10) and 317.4 m^2 g^{-1} for the thermally activated sample—TK10.

Thermal activation of montmorillonite TK10 changes its sorption properties, structure, and composition. This is a method of physical modification K10. The process of thermal activation of MMT is characterized by four reactions: (1) dehydration (about 220 °C) (2) dehydroxylation (350–1000 °C), (3) decomposition and (4) recrystallization [15]. The crystal structure of MMT-K10 is disturbed by the processes listed under (a) and (b).

On the other hand, activating clay with a high concentration of inorganic acids is a method of chemical modification of clay. The principle of the method is based on the replacement of exchangeable clay cations with H^+, Al^{3+} and other ions that can be released from octahedral and tetrahedral layers, where SiO_4 groups of tetrahedral layers generally remain intact. The process of activating clay with acids can be divided into three phases. In the first phase, the

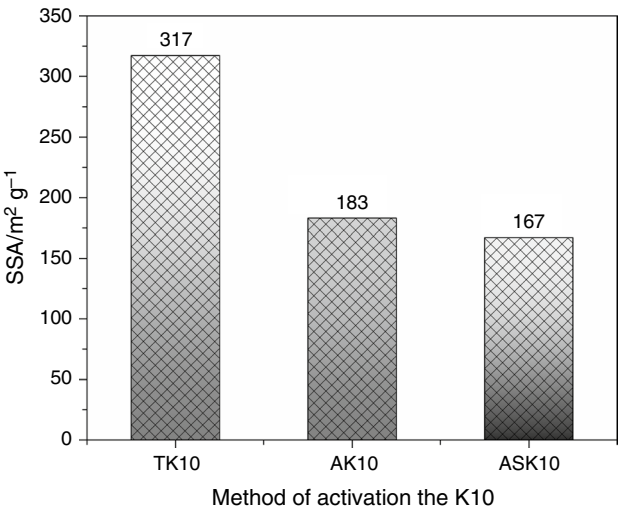

Fig. 1 Influence of method of activation of the K10 on the SSA

process that occurs is the ion exchange of the cation of the interlayer space of clay with H^+ acid ions, while preserving the crystal structure of the clay. In the next phase, due to a longer contact time and a higher concentration of H^+ ions, the structure of the octahedral layers of clay is disturbed due to the exchange of octahedral cations with H^+ acid ions. In the last phase, there is a complete disruption of the crystal structure of the clay, which is a consequence of the action of the acid on the tetrahedral layers; the result is the formation of an amorphous phase [18]. Acid activation of clay achieves an increase in SSA, porosity, and acidity of clay minerals as well as partially removing inorganic impurities and dissolving the outer layers clay minerals [28]. The degree of change in the active surface and the porosity of the clay structure created by the action of acids depends on the type of clay mineral, i.e. the chemical composition of clay, types of interlayer cations, applied acid and its concentration, temperature, and time of action [29]. Four parameters, such as temperature, contact time, the mass percentage of acid, and solid–liquid ratio strongly influence the structural properties [30]. This process causes an increase in the SSA, acidity, it introduces permanent mesoporosity [31], and removes metal ions from the crystal layer, which partially stratifies the clay. The decrease in SSA in the sample that was subsequently activated by the magnetic stirrer can be explained by the subsequent collapse of the already weakened K10 crystal lattice by mechanical means.

The obtained results (Fig. 1) show that the activation of montmorillonite K10 was successfully performed because there was an increase in SSA in all modified samples. The highest degree of activation is, judging by the value for SSA determined by the Sear's method, in the thermally activated sample TK10 and is 317.4 $m^2\ g^{-1}$. The higher value of the specific surface area, obtained by the Sear's method, indicates that TK10 has a larger number of silanol groups that are capable of reacting with formaldehyde from UF resins. Furthermore, such a high value for TK10 may be due to the deprotonation of internal silanol groups by NaOH because the OH^- ion is smaller than the nitrogen atom in BET determination of SSA, and can penetrate micropores [32].

XRD, SEM, crystallinity, FTIR, and TG/DTA investigation of differently activated K10

Nandiwale and co-authors [33] as well as Marsh et al. [34] determined that unmodified sample K10 contains clays, muscovite and quartz, while feldspar and kaolin can be found in small percentages. The primary phase of K10 is muscovite while the secondary phase is montmorillonite [35].

Figure 2 shows XRD patterns for different activated montmorillonite K10.

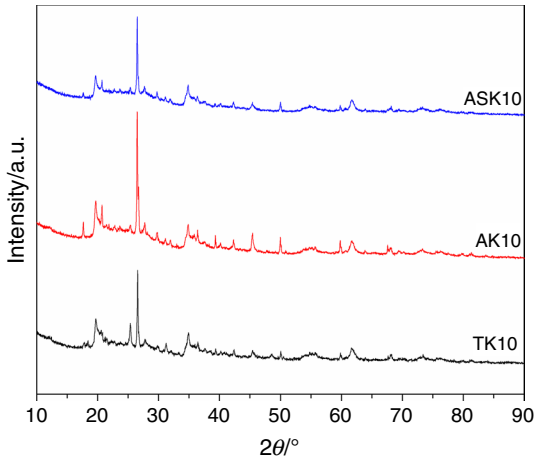

Fig. 2 X-ray diffractograms of differently modified K10

Table 1 Crystallinity and average crystallite size (*D*) of modified K10 and synthesized modified γ-irradiated UF/K10 composites

Samples	Crystallinity/%	Average crystallite size-*D*/nm
TK10	75.48	15.74
AK10	82.75	18.97
ASK10	78.15	19.55
UF/TK10	75.03	14.54
UF/AK10	73.04	16.30
UF/ASK10	78.04	16.13

We can observe that peaks at 2θ with values of 26.6°, 26.4°, and 26.4° originate from quartz for TK10, AK10, and ASK10 [34]. The intensity of the peaks decreases with the mode of activation of K10 and this is in accordance with the results obtained for crystallinity (Table 1). The highest crystallinity of 82.75% is shown by the sample activated by sulfuric acid-AK10. The partially layered structure in the case of the AK10 was converted into plate particles for ASK10 resulting in a disordered structure consistent with the results for the morphology of the studied samples (Fig. 3b, c). Since the difference in activation between AK10 and ASK10 samples is only in the application of the stirrer, it was to be expected that the crystallinity decreased further due to additional collapse of the crystal structure due to the mechanical stirrer and this is clearly seen in the morphology of the samples (Fig. 3b, c).

FTIR spectra and the corresponding data of modified K10 are presented in Fig. 4 and Table 2. The FTIR spectra of modified K10 samples exhibited a sharp band centered about 1030 cm^{-1}, which is characteristic for stretching vibrational mode of a –Si–O bond of quartz, in-plane. A small band at 910 cm^{-1} can be assigned to the Al–Al–OH bending

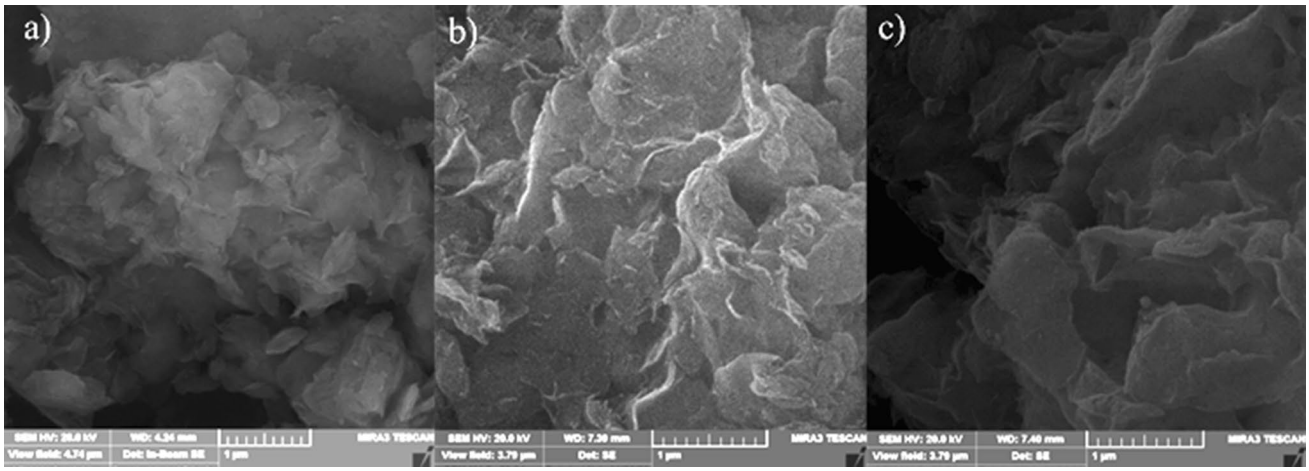

Fig. 3 SEM micrographs of **a** TK10, **b** AK10 and **c** ASK10 with magnification at ×50,000

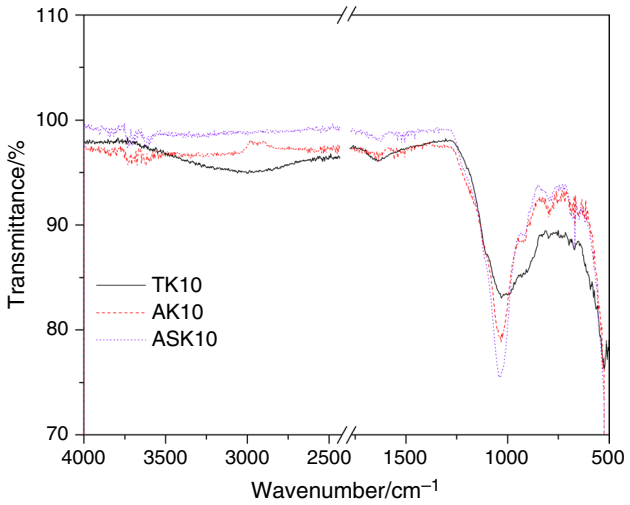

Fig. 4 FTIR spectra of differently modified montmorillonite K10

vibrations of aluminates. The bands around about 790 cm^{-1} and around 660–680 cm^{-1} are attributed to stretching vibrations of –Si–O of quartz and of –Si–O group [27, 36]. The small band at 1636 cm^{-1} is characteristic of deformation vibrations of the hydroxyl groups in molecular water are noticed. The bands at 3716 cm^{-1} and 3712 cm^{-1} and around 3610 cm^{-1} show the presence of hydroxyl linkage in clay in FTIR spectra of AK10 and ASK10 samples. These two bands show that the hydroxyl group is coordinated with octahedral cations such as Al^{3+} and Mg^{2+} [37]. The band at 571 cm^{-1} is due to Al–O–Si bending vibrations. The peak around 790 cm^{-1} belongs to stretching vibration of Si–O–Fe. The broadband in FTIR spectra of TK10 sample at 3033 cm^{-1} and 1636 cm^{-1} characterize stretching vibrations of –OH, and the –OH in molecular water (H–OH deformation) are detected. The peak at 796 cm^{-1} belongs to stretching vibration of Si–O–Fe, and 526 cm^{-1} for bending vibration of Si–O–Mg, respectively [15, 38].

Variations in the frequency and intensity of the most intense peak in the FTIR spectrum located at about 1000 cm^{-1} range from 1027 cm^{-1} for TK10, 1032 cm^{-1} for AK10, and 1034 cm^{-1} for ASK10, and are about 11 cm^{-1}. This data is very important because it shows that the peak attributed to Si–O valence vibrations is sensitive to the close environment associated with the clay structure. A similar observation is made by Ahmed and et al., in their work [37].

In Fig. 5 we can see a comparison of the TGA/DTG (a), and DTA (c) curves of differently treated montmorillonite; TK10, AK10, and ASK10, respectively. Table 3 shows the characteristic values of mass loss for modified K10 and modified UF/K10 composites. Based on the data from Fig. 5a and Table 3, it can be seen that all three tested samples have multi-stage processes that additionally overlap (some of them). For example, in the case of the TK10 sample, it is a four-stage degradation reaction, with several reactions taking place simultaneously in the first stage, which is marked with an asterisk in Table 3. In the case of AK10 and ASK10 samples, the degradation reaction is two-stage, but there are also several reactions that overlap in the second stage of degradation.

The first step decomposition, temperature area, 30–346.6 °C for TK10 sample and with DTG maximum at 96.8, 199.2 and 272.9 °C (Table 3) which overlap with each other. The mass loss for TK10 is 11.7%. Dehydration occurs at temperatures up to 300 °C, releasing adsorbed and exchangeable water coordinated by the cation [39, 40]. Mass losses in the second (370.6–505.9 °C) and third step of degradation (517.9–645.9 °C) are 1.7% and 3.3%, which correspond to the dehydroxylation of the montmorillonite phase. The corresponding DTG peaks are located at 469.8 °C and 596.2 °C. The fourth degradation step, which takes place in

Table 2 Characteristic IR bands of modified K10 and modified γ-irradiated UF/K10 composites and its possible assignation

Samples Wave number/cm^{-1}						Assignment
TK10	AK10	ASK10	UF/TK10	UF/AK10	UF/ASK10	
–	3716	3712	3733	3733	3733	ν(OH) coordinated with OH cation, and ν(OH) in Al–Al–OH and Al–OH–Mg fragments in MMT
–	3612	3608	3627	3645	3646	ν(Al–OH)
–	–	–	3310	3331	3316	ν(NH) in 2°-amine and hydrogen bonded O–H
2991	–	–	–	–	–	ν(OH) and δ(H–OH) in H_2O
1636	1636	1634	1631	1636	1636	ν(C=O) in $–CONH_2$ (amide I) and δ(OH) in water
–	1530	1525	1559	1557	1557	δ(NH) in NH–CO in 2°-amine (amide II)
–	–	–	1380	1385	1385	δ(CH) in CH_2/CH_2OH/N–CH_2–N; δ(CH_2)
–	–	–	1241	1244	1244	ν_{as}(C–C–O); ν(N–CH_2–N) in 2°-amine; ν_{as}(C–O–C)
1027	1031	1038	1136	1133	1133	ν(–Si–O) of quartz; ν(C–N) group in the methylene bond (HNCH_2NH)
–	–	–	1034	1036	1033	ν(–Si–O) of quartz; ν_{as}(N–CH_2–N), ν(C–O–C) of ether linkage, organic siloxane or silicone ν(Si–O–C), ν(Si–O–Si) in MMT;
912	910	910	934	948	934	δ(Al–Al–OH)
796	790	796	772	778	774	ν(Si–O) of quartz; (Al–Si) in MMT; ν(Si–O–Fe)
679	658	663	669	669	669	ν(Si–O); γ(Al–O); γ(Si–O) in MMT
526	571	571	511	511	519	γ(Al–O–Si) in MMT, γ(Si–O–Mg) in MMT

ν-stretching vibrations, δ-bending vibration in plane, γ-bending vibration out to plane

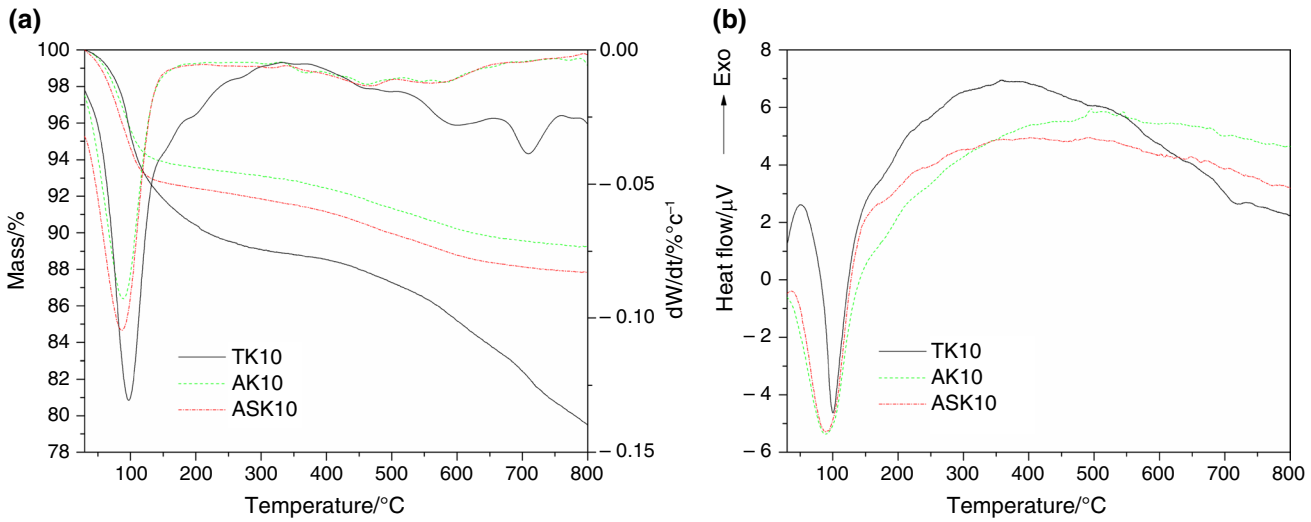

Fig. 5 TGA/DTG curve (**a**) and DTA curve (**b**) of differently activated K10

the temperature range of 653.3–800 °C with a corresponding DTG peak at 712.0 °C and a mass loss of 3.5%, originates from the dehydroxylation of the crystal lattice structure of the K10 layer [41].

The thermal behavior of modified AK10 and ASK10 contains two main mass loss processes (Fig. 5a, Table 3). The mass loss of modified AK10 and ASK10 occurs in the similar temperature ranges at 30–202.2 °C and 30–179.7 °C with DTG peaks at 89.7 °C for AK10 and 91.1 °C for ASK10. The mass loss in that step is 6.4 and 7.4% for AK10 and ASK10. These mass losses originate from the loss of adsorbed water. Second step degradation occurs in temperature intervals at 328.4–800 °C and 339.0–800 °C (with DTG peaks at 364.5, 459.4, 545.1 and 582.6 °C for AK10 and 468.4, and 573.7 °C for ASK10). The mass loss in these steps is 4.3 and 4.7%. From Fig. 5a the second degradation step is obvious by four and two overlaping peaks for AK10 and ASK10, respectively. Dehydration occurs at temperatures up to 300 °C when adsorbed and exchangeable water coordinated with the cation is released. Dehydroxylation

Table 3 DTG, DTA data of peak values, temperature intervals, $T_{5\%}$ and mass loss from modified K10 and modified UF/K10 composites

Samples	Temperature interval/°C	DTG peak values/°C	Mass loss/%	DTA endothermic peak value/°C	$T_{5\%}$/°C	Total mass loss/%
TK10		96.8*	11.7*		69.1	20.5
	30–346.6*	199.2*		100.7		
	370.6–505.9	272.9*		179.3		
	517.9–645.9	469.8	1.7	492.7		
	653.3–766.2	596.2	3.3	718.1		
		712.0	3.5			
AK10		89.4	6.4		52.4	10.8
	30–202.2	364.5*	4.3*	89.7		
	328.4–800*	459.4*		181.4		
		545.1*		697.1		
		582.6*				
ASK10		86.4	7.4	91.1	46.6	12.2
	30–179.7	468.4*	4.7*	188.9		
	339.0–800*	573.7*		459.6		
UF/TK10	30–123.9	83.4	7.0	92.7	96.9	61.4
	129.9–185.7	157.1	3.1	158.8		
	196.1–391.73*	254.8*	33.9*	256.6		
	552.7–657.9	278.9*		285.1		
	678.9–800	618.8	11.6	479.1		
		721.0	5.7			
UF/AK10	30–157.1	92.8	4.4		103.2	53.2
	175.1–406.7	257.9	38.8	91.1		
	439.9–689.5	558.9	7.8	259.6		
	740.6–800	764.7	1.0	453.6		
UF/ASK10	30–161.5	93.8	4.7	91.1	101.2	54.9
	173.7–409.0	256.4	38.7	173.9		
	704.6–800	742.2	11.6	259.6		

*Overlapping peaks and the corresponding total mass loss

occurs in the temperature range 400–750 °C, while at a high temperature > 800 °C, a new phase is formed by crystallization from dehydroxylated clay (thermostable aluminosilicate minerals) [39, 40].

The total mass loss for TK10 is 20.5% for AK10 is 10.8%, and for ASK10 is 12.2%. Based on the value for $T_{5\%}$ it can be said that the sample TK10 is the most stable because its degradation begins at a temperature of 69.1 °C while the other two samples begin to degrade at 52.4 °C (AK10) and 46.6 °C (ASK10) (Table 3). These results show that the modification of K10 with sulphuric acid disrupts its structure and is further disrupted by stirring on a magnetic stirrer, so the mass loss is greater in the sample, which after chemical activation is further activated by stirring.

Figure 5b shows a DTA peak of the TK10 at 100.7 °C with a shoulder at 179.3 °C originating from the evaporation of adsorbed water and exchangeable water. The second peak-shoulder at 179.3 °C is caused by the removal of interlayer water from montmorillonite. A higher temperature is required to remove the interlayer water because –OH bonds are formed between H atoms of water and O atoms from the Si–O surface K10 [42]. The following endothermic DTA peaks located at 492.7 °C and 718.1 °C originate from dehydroxylation of the TK10.

In the case of AK10 and ASK10 samples, the endothermic peaks resulting from the evaporation of the adsorbed water are located at 89.7 °C and 91.1 °C. The endothermic peaks at 181.4 °C and 188.9 °C belong to AK10 and ASK10, respectively, and originate from the evaporation of interchangeable water. Due to the higher amount of O–H bond and bond energy between water and the surface of the montmorillonite layer, there will be a higher water removal temperature. The number of O–H bonds and adsorption energy increase with increasing charge density leading to an increase in the dehydration temperature of montmorillonite [41]. Since the dehydroxylation process takes place in the temperature range 400–750 °C, then the DTA peaks in that temperature range originate from it

(DTA peaks at 492.7 and 718.1 °C for AK10 and 697.1 °C for ASK10, respectively).

Characterisation of modified γ-irradiated UF/K10 composites

UF resins are formed by polycondensation reactions between urea and formaldehyde. By different reaction conditions and methods of synthesis, it is possible to obtain a large number of condensation structures: from the simplest monomethylolureas to the most complex three-dimensional crosslinked polymers. UF resins are used in the wood industry, where they are more prevalent compared to other resins, such as phenol–formaldehyde resins. The reason for this is the numerous positive properties, which are reflected in high reactivity, fast curing, good performance on wood board, as well as low cost.

One of the most prominent solutions for improving the properties of UF resins is to reduce the *F*/*U* ratio. Literature data [43, 44] show that UF resins with a lower *F*/*U* molar ratio reduce the content of methylol groups and branching of the structure, which leads to lower water sorption, stronger bonding between chains and other side effects. However, there is a problem in the form of reducing the reactivity of UF resins, which affects the poorer quality of the produced plates [45].

The XRD patterns for γ-irradiated modified UF/K10 composites are shown in Fig. 6. The crystallinity of modified γ-irradiated UF/K10 resins was shown in Table 1.

Peaks with maximum at 2θ of 20.59°, 22.24°, and 24.19° in the modified γ-irradiated UF/TK10, and 20.75°, 22.4°, and 23.59° in the modified γ-irradiated UF/AK10 composite and at 20.75°, 22.24°, and 23.45° in the modified γ-irradiated UF/ASK10 are typical for the samples UF, which is in accordance with the literature data [46]. As a consequence of the increase in the *d*-spacing, the peaks move from higher to lower 2θ values in accordance with Bragg's law [47]. By comparing 2θ characteristic values for UF resin in modified γ-irradiated UF/K10 composites, we see that the d-spacing changes depending on the way K10 itself is modified. All modified UF composites showed typical diffraction peaks of pure UF resin which is attributed to the layered structure of CO-HN formed from the carboxyl group (O-ligand) and the amine group (N-ligand) [48].

The intensity of the characteristic peak at 26.59°, which belongs to quartz, has maintained the same downward trend as with the modified K10 (Fig. 2).

Based on the data from Table 1, it can be seen that UF/ASK10 composite shows the highest value for crystallinity at 78.04%. The order of decreasing crystallinity is: UF/ASK10 > UF/TK10 > UF/AK10. Crystal domains are made of arranged packaging of linear molecules of low molar UF resins due to the interaction of H-bonds that can potentially inhibit branching and crosslinking [49].

FTIR spectra of modified γ-irradiated UF/K10 composites are shown in Fig. 7. The characteristic bands of modified UF/K10 composites in FTIR spectra are shown in Table 2.

A sharp but small doublet occurring at around 3630–3650 cm^{-1} and at 3733 cm^{-1} indicates –O–H stretching vibrations in the Al–Al–OH and Al–OH–Mg fragments of the MMT in all modified UF/K10 composites. The wideband at 3310, 3331, and 3316 cm^{-1} from the spectra UF/TK10, UF/AK10, and UF/ASK10, respectively, belong to stretching vibrations of secondary amides (N–H). The peaks around 1630 cm^{-1} and around 1560 cm^{-1} for all modified UF/K10 composites were attributed to the stretching of the carbonyl group (>C=O) and –CN stretching of secondary amines, respectively [50]. It can be clearly seen from Table 2 that the band originating from the vibrations C=O moves

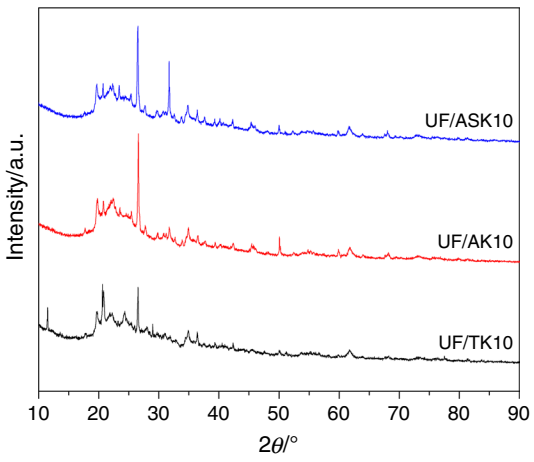

Fig. 6 X-ray diffractograms of modified γ-irradiated UF/K10 composites

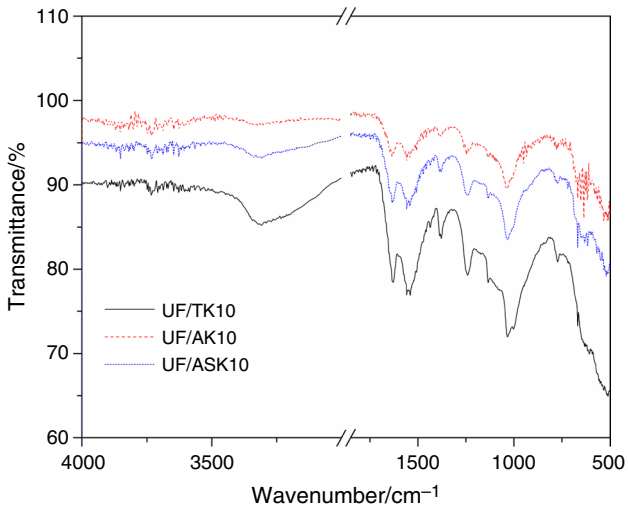

Fig. 7 FTIR spectra of modified γ-irradiated UF/K10 composites

towards a larger wave number (from 1630 to 1634 cm^{-1}) by changing the activation mode K10. Accordingly, the N–H band also moved from 3310 cm^{-1} to 3331 cm^{-1} and 3315 cm^{-1}, which indicates that the H-bonds in the hardened low molar modified γ-irradiated UF/K10 composites disappeared mainly due to the formation of crosslinked structures [51]. Figure 7 shows the intensity of the bands at around 1386 cm^{-1} and 1130 cm^{-1}, that are attributed to the vibrations of the hydroxymethyl ($HOCH_2NH$-) and ether bonds ($HNCH_2OCH_2NH$-) decreases, depending on which activation method of the K10 was applied. The decrease in the intensity of peak around 1130 cm^{-1} was accompanied by an increase in the peak around 1036 cm^{-1} resulting from vibrations of the C-N group in the methylene bond ($HNCH_2NH$). Based on the work of Wibowo et al. [52] it could be concluded that the addition of K10 caused crosslinking, which would ultimately improve the adhesion strength of UF resins. A peak around 510–520 cm^{-1} attributed to Si–O–Si vibrations and Si–O–Mg deformation vibrations in K10 indicates that K10 is incorporated into the UF resin. As can be seen in FTIR spectra, the consequence of forming a multi-branched structure in modified UF resins, which formulate more methylene bonds (–$HNCH_2NH$–) at about 1240 cm^{-1} via K10 intercalation, results in lower crystallinity in modified UF resins which is in agreement with the results obtained for crystallinity (Table 1). Stretching vibrations of the following adsorption bands were detected in FTIR spectra for modified UF/K10 composites: around at 1240 cm^{-1} for –CN; –N–H of 3° amines, –C–O–C– in ether bonds [53]; 1560 cm^{-1} for –N–H; 1630 cm^{-1} for –NH–CO, and 3310 cm^{-1} for –NH. The other observed peaks around 1107 cm^{-1} and around 1030 cm^{-1} were assigned to –C=O aliphatic ether and methylene bridge (N–CH_2–N), respectively [46]. A weak band around 1380–1385 cm^{-1} is attributed to the deformation vibrations of the CH group in CH_2/CH_2OH/N-CH_2-N. This peak illustrates the typical reaction between urea and formaldehyde.

The TGA spectrum of modified γ-irradiated UF/K10 composites represents in Fig. 8. Table 3 shows the values for DTG and DTA peaks, temperature intervals, total mass loss and values of the T_5% from modified γ-irradiated UF/K10 composites.

The addition of layered fillers can affect the thermal stability of the polymer. The filler acts as a strong thermal insulator, as a barrier for the evaporation of volatile degradation products from the sample or may contribute to the formation of soot after the initial stage of thermal degradation. Two important papers provide an overview of the thermal properties and decomposition processes of composites based on different polymer matrices [54, 55]. They consider the basic changes in the thermal behavior of different polymer matrices after the addition of montmorillonite, with special emphasis on the influence of montmorillonite on the kinetics of the decomposition process and the formation of condensed/volatile products under oxidative and pyrolytic conditions. The results of recent research recorded in the mentioned and other works [56–58] indicate that the introduction of layered silicates into the polymer matrix causes an increase in thermal stability.

Figure 8a clearly shows that in all modified γ-irradiated UF/K10 composites the degradation takes place in several stages, in UF/TK10 it takes place in five steps, in UF/AK10 in four, and in UF/ASK10 in three steps.

The mass loss observed below 200 °C in all modified samples irradiated with gamma rays UF/K10 composites materials is attributed to the loss of adsorbed water and formaldehyde release and is accompanied by a small DTA endothermic peak below 100 °C (Fig. 8b). Mass losses at

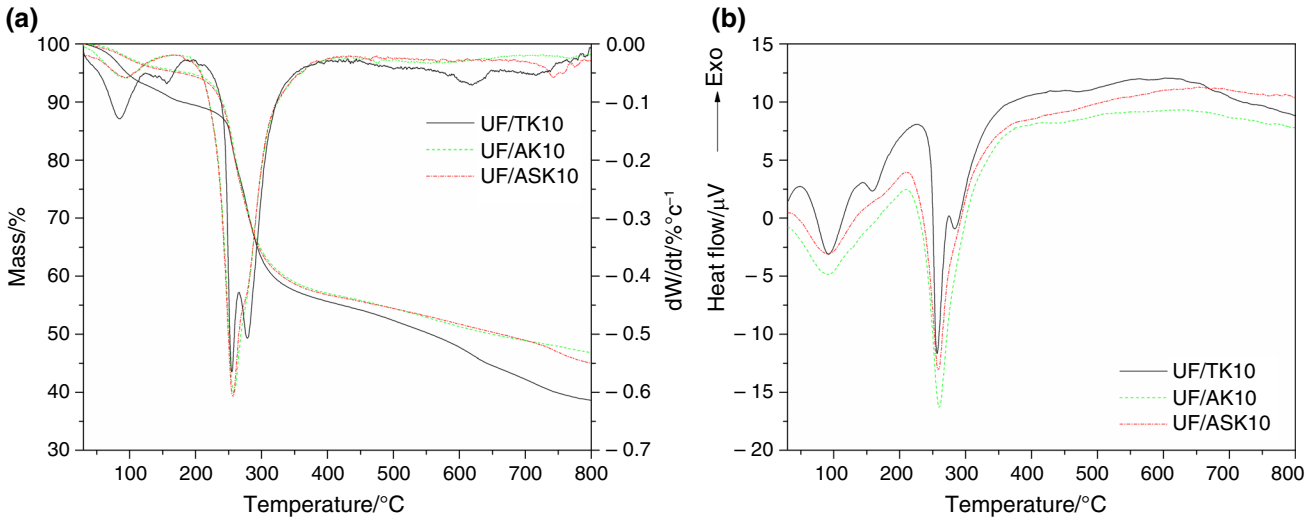

Fig. 8 TGA/DTG curve (**a**) and DTA curve (**b**) modified γ-irradiated UF/K10 composites

this stage are 7%, 4.4%, and 4.7% for UF/TK10, UF/AK10, and UF/ASK10, respectively (Table 3), as confirmed by DTA endothermic peaks with a minimum at 92.7 for UF/TK10 and 91.1 °C for UF/AK10 and UF/ASK10 composites, respectively.

The second degradation step for UF/TK10 occurs in the temperature range 129.9–185.7 °C with a mass loss of 3.1% and with a DTG peak at 157.1 °C. This value refers to condensed water formed during subsequent curing, but also to adsorbed and interchangeable water [59, 60]. Confirmation of this is the existence of DTA peaks with a minimum at 158.8 °C (Fig. 8b).

Degradation of cross-linked resins begins with the release of formaldehyde from dimethylene-ether bonds, and the highest rate of degradation is achieved when stable methylene-ether bonds are broken [61–63]. The main mass loss occurs at this stage.

This degree of degradation for modified UF/TK10 composite (the third degradation step) takes place in two stages that overlap each other in the temperature range of 196.1–391.73 °C. This means that in this stage, two degradation processes take place simultaneously and one peak with a "shoulder" is obtained, which is the top of the other peak. The DTG values of the peaks of these two processes are 254.8 °C and 278.9 °C. The mass loss for these two overlapping degradation processes is 33.9%. The presence of DTA peaks (Fig. 8b) located at 256.6 °C and 285.1 °C are the result of the degradation of methylene-ether bonds and the crosslinking reaction in the resin network. For modified UF/AK10 and UF/ASK10 composites, this degradation process (second degradation step) occurs in almost the same temperature range of about 170–410 °C (Table 3). The mass losses are also almost identical and amount to 38.8% and 37.7%, while the DTG peak values are 257.9 °C and 282.1 °C for the modified UF/AK10 and 256.4 °C and 277.5 °C for UF/ASK10 composites, respectively. The DTA peaks for these two composites are at identical values and amount 259.6 °C.

The fourth step of degradation beginning at 552.7 °C and terminate at 657.9 °C, for UF/TK10 composite. The mass loss expressed as a percentage in this step degradation is 11.6%. According to previous work of Samaržija-Jovanović et al. [27], DTG peaks at 618.8 °C belong to the dehydration of silanol groups in the particles of modified K10 that cause mass loss from 11.6%. In the case of the modified UF/AK10 composite, the third degradation step occurs in the temperature range 439.9–689.5 °C with a DTG minimum at 558.9 °C and a mass loss of 7.8%. As with the modified UF/TK10 composite, it is a matter of dehydration of silanol groups on the surface K10. The presence of DTA endothermic peaks at 479.1 °C and 453.6 °C for UF/TK10 and UF/AK10 composites confirms this. The final degradation steps start at 678.9 °C, 740.6 °C, and 704.6 °C and end at 800 °C for modified UF/TK10, UF/AK10, and UF/ASK10 composites. The mass losses for this degradation step are 5.7%, 1%, and 11.6%. The total mass loss for modified UF/TK10, UF/K10 and UF/ASK10 composites are 61.4, 53.2, and 54.9% respectively. DTG peaks located at 721.0 °C, 764.7 °C, and 742.2 °C in modified UF/TK10, UF/AK10 and UF/ASK10 composites are due to dehydroxylation of K10.

The $T_{5\%}$, values lead to the conclusion that the modified UF/AK10 composite has better thermal stability than the UF/TK10 and UF/ASK10 composites because its degradation begins starts at a higher temperature of 103.2 °C compared to 96.9 °C and 101.2 °C. The increase in thermal stability of the modified UF/AK10 composite was attributed to the better dispersion of silicate layers, which prevented the diffusion of heat into macromolecules [63].

Conclusions

The influence of different modification K10 on the thermal stability of modified γ-irradiated UF/K10 composites has been investigated and has led to the following conclusions:

Montmorillonite K10 has been successfully activated using calcination TK10, sulfuric acid AK10 and sulfuric acid and by stirring on a magnetic stirrer ASK10, as shown by FTIR, XRD, and TGA studies, which is proved by the increase in the specific surface area. XRD analysis shows that the percentage of crystallinity decreases with the mode of activation of K10 from 82.75% to 78.15% for AK10 and ASK10, and to 75.48% for TK10, respectively. The degree of crystallinity is the lowest at UF/AK10 composite and is 73.04%. The shift of N–H bands from 3310 cm^{-1} (UF/TK10) to 3331 cm^{-1} (UF/AK10) and 3315 cm^{-1} (UF/ASK10), indicates that the disappearance of H-bonds in modified γ-irradiated UF/K10 composites and a decrease in intensity is mainly due to the formation of crosslinked structures. The intensity of the bands at around 1380–1386 cm^{-1} from modified γ-irradiated UF/TK10 composite belonging to the vibrations from -CH_2OH decreases rapidly (disappears) and has the lowest intensity in UF/AK10 composite, which is attributed to the reduction of -CH_2OH groups. Based on the values for $T_{5\%}$ (103.2 °C) it can be concluded that the modified γ-irradiated UF/AK10 composite has better thermal stability than other composites.

Acknowledgements The research was funded by the Ministry of Education, Science and Technological Development of the Republic of Serbia (contract number 451-03-68/2022-14/200123 and 451-03-68/2022-14/ 200017).

Author contributions SS-J: Conceptualization, Methodology, Investigation, Writing-review & editing, Supervision. VJ: Investigation, Writing-original draft, Project administration. TJ: Investigation, Validation. BP: Investigation, Writing-original draft, Writing-review & editing, Visualization. GM: Investigation, Writing-review & editing,

SP: Investigation, Validation MM-C: Resources, Investigation, Writing-original draft, Writing-review & editing, Visualization.

Funding The research was funded by the Ministry of Education, Science and Technological Development of the Republic of Serbia (Contract Number 451-03-68/2022-14/200123 and 451-03-68/2022-14/200017).

Data availability Not applicable.

Code availability Not applicable.

Declarations

Conflict of interest Authors have not any actual or potential conflict of interest including any financial, personal or other relationships with other people or organizations.

Ethical approval Not applicable.

Consent to participate The article has been written by the stated authors who are ALL aware of its content and approve its submission.

Consent for publication All mentioned authors agree that the paper should be published if the paper is accepted for publication.

References

1. Park BD, Causin V. Crystallinity and domain size of cured urea–formaldehyde resin adhesives with different formaldehyde/urea mole ratios. Eur Polym J. 2013;49:532–7. https://doi.org/10.1016/j.eurpolymj.2012.10.029.
2. Dunky M. Urea-formaldehyde (UF) Adhesive Resins for Wood. Int J Adhes Adhes. 1998;18:95–107. https://doi.org/10.1016/S0143-7496(97)00054-7.
3. Conner AH. Urea-formaldehyde adhesive resins. In: Salamone JC, editor. Polymeric materials encyclopedia. New York: CRC Press; 1996.
4. Jeong B, Park BD. Effect of molecular weight of urea-formaldehyde resins on their cure kinetics, interphase, penetration into wood, and adhesion in bonding wood. Wood Sci Technol. 2019;53:665–85. https://doi.org/10.1007/s00226-019-01092-1.
5. Jovanović V, Samaržija-Jovanović S, Petković B, Miličević Z, Marković G, Marinović-Cincović M. Biocomposites based on cellulose and starch modified urea-formaldehyde resin: hydrolytic, thermal, and radiation stability. Polym Compos. 2019;40:1287–94. https://doi.org/10.1002/pc.24849.
6. Pizzi A, George B, Zanetti M, Méausoone P. Rheometry of aging of colloidal melamine-urea-formaldehyde polycondensates. J Appl Polym Sci. 2005;96:655–9. https://doi.org/10.1002/APP.21492.
7. Kim JW, Carlborn K, Matuana LM, Heiden P. Thermoplastic modification of urea–formaldehyde wood adhesives to improve moisture resistance. J Appl Polym Sci. 2006;101:4222–9. https://doi.org/10.1002/app.23654.
8. Usuki A, Kojima Y, Kawasumi M, Okada A, Fukushima Y, Kurauchi T, Kamigaito O. Synthesis of nylon 6-clay hybrid. J Mater Res. 1993;8(5):1179–84. https://doi.org/10.1557/JMR.1993.1179.
9. Bauer F, Glasel HJ, Hartmann E, Langguth H, Hinterwaldner R. Functionalized inorganic/organic nanocomposites as new basic raw materials for adhesives and sealants. Int J Adhes Adhes. 2004;24:519–22. https://doi.org/10.1016/j.ijadhadh.2004.02.001.
10. Lee WF, Yang LG. Superabsorbent polymeric materials. XII. Effect of montmorillonite on water absorbency for poly (sodium acrylate) and montmorillonite nanocomposite superabsorbents. J Appl Polym Sci. 2004;92(5):3422–9. https://doi.org/10.1002/app.20370.
11. Moore DM, Reynolds RC Jr. X-ray diffraction and the identification and analysis of clay minerals. 2nd ed. Oxford: Oxford University Press; 1997.
12. Guggenheim S, Adams JM, Bain DC, Bergaya F, Brigatti MF, Drits VA, Formoso MLL, Galán E, Kogure T, Stanjek H. Summary of recommendations of nomenclature committees. Relevant to clay mineralogy: Report of the Association Internationale Pour L'etude des Argiles (AIPEA) Nomenclature Committee for 2006. Clays Clay Miner. 2006;54:761–72. https://doi.org/10.1346/CCMN.2006.0540610.
13. Wilson MJ. Rock-forming minerals. Sheet silikates: clays minerals. London: The Geological Society; 2013.
14. Krupskaya V, Zakusin S, Tyupina E, Dorzhieva O, Zhukhlistov A, Belousov P, Timofeeva M. Experimental study of montmorillonite structure and transformation of its properties under treatment with inorganic acid solutions. Minerals. 2017;7:49–64. https://doi.org/10.3390/min7040049.
15. Zuo Q, Gao X, Yang J, Zhang P, Chen G, Li Y, Shi K, Wu W. Investigation on the thermal activation of montmorillonite and its application for the removal of U(VI) in aqueous solution. J Taiwan Inst Chem Eng. 2017;80:757–60.
16. Wypych F. In: Wypych F, Satyanarayana GK, editors. Clay surfaces: fundamentals and applications, vol. 1. London: Academic Press; 2004.
17. Önal M, Sarıkaya Y. Preparation and characterization of acid-activated bentonite powders. Powder Technol. 2007;172:14–8. https://doi.org/10.1016/j.powtec.2006.10.034.
18. Komadel P, Madejová J. In: Bergaya F, Theng BKG, Lagaly G, editors. Handbook of clay science. 1st ed. Amsterdam: Elsevier Ltd; 2006.
19. Marković G, Samaržija-Jovanović S, Jovanović V, Budinski-Simendić J, Marinović-Cincović M. Gamma irradiation: properties, behavior and applications. In: Brock J, editor. Gamma irradiation: properties, effects and development of new materials. New York: Nova Science Publisher; 2021.
20. Ajemba RO. Kinetics and equilibrium modeling of lead(II) and chromium(III) ions' adsorption onto clay from Kono-bowe. Nigeria Turkish J Eng Environ Sci. 2014;38:455–79. https://doi.org/10.3906/muh-1402-3.
21. Stoiljković S, Todorović B. Adsorption-desorption and usable properties of bentonite-based materials. Leskovac: Monografy (in Serbian Lanque); 2018.
22. Jovanović V, Samaržija-Jovanović S, Petković B, Dekić V, Marković G, Marinović-Cincović M. Effect of γ-irradiation on the hydrolytic and thermal stability of micro- and nano-TiO_2 based urea-formaldehyde composites. RSC Adv. 2015;5:59715–22. https://doi.org/10.1039/C5RA10627C.
23. Marković VM, Eymery R, Yuan HC. A new approach of Co-60 plant design for introduction of radiation sterilization in developing countries. Radiat Phys Chem. 1977;9(4–6):625–31. https://doi.org/10.1016/0146-5724(77)90176-5.
24. Sears GW. Determination of specific surface area of colloidal silica by titration with sodium hydroxide. Anal Chem. 1956;28:1981–1883. https://doi.org/10.1021/ac60120a048.
25. Wibowo E, Park BD. Determination of crystallinity of thermosetting urea-formaldehyde resins using deconvolution method. Macromol Res. 2020;28(6):615–24. https://doi.org/10.1007/s13233-020-8076-2.

26. Kordkheili HY, Najafi SK, Behrooz R. Influence of nanoclay on urea–glyoxalated lignin–formaldehyde resins for wood adhesive. J Adhes. 2017;93(6):431–43. https://doi.org/10.1080/00218464.2015.1079521.
27. Samaržija-Jovanović S, Jovanović V, Petković B, Jovanović T, Marković G, Porobić S, Papan J, Marinović-Cincović M. Hydrolytic, thermal, and UV stability of urea-formaldehyde resin/thermally activated montmorillonite nanocomposites. Polym Compos. 2020;41(9):3575–84. https://doi.org/10.1002/pc.25644.
28. Rusmin R, Sarkar B, Biswas B, Churchman J, Liu Y, Naidu R. Structural, electrokinetic and surface properties of activated palygorskite for environmental application. Appl Clay Sci. 2016;134:95–102. https://doi.org/10.1016/j.clay.2016.07.012.
29. Bhattacharyya KG, Gupta SS. Adsorption of a few heavy metals on natural and modified kaolinite and montmorillonite: a review. Adv Colloid Interface Sci. 2008;140:114–31. https://doi.org/10.1016/j.cis.2007.12.008.
30. Amari A, Gannouni H, Khan MI, Almesfer MK, Elkhaleefa AM, Gannouni A. Effect of structure and chemical activation on the adsorption properties of green clay minerals for the removal of cationic dye. Appl Sci. 2018;8:2302–32. https://doi.org/10.3390/app8112302.
31. Razzaghi-Kashani KM, Hasankhani H, Kokabi M. Improvement in physical and mechanical properties of butyl rubber with montmorillonite organo-clay. Iran Polym J. 2007;16(10):671–9.
32. Oertel T, Hutter F, Helbig U, Sextl G. Amorphous silica in ultra-high performance concrete: first hour of hydration. Cem Concr Res. 2014;58:131–42. https://doi.org/10.1016/j.cemconres.2014.01.008.
33. Nandiwale KY, Niphardar PS, Bokade VV. Synthesis of oxygenated fuel additives via acetylation of bio-glycerol over H_2SO_4 modified montmorillonite K10 catalyst. Prog Petrochemical Sci. 2018. https://doi.org/10.31031/PPS.2018.01.000501.
34. Marsh A, Heath A, Patureau P, Evernden M, Walker P. Alkali activation behaviour of un-calcined montmorillonite and illite clay minerals. Appl Clay Sci. 2018;166:250–61. https://doi.org/10.1016/j.clay.2018.09.011.
35. Jiang JQ, Zeng Z. Comparison of modified montmorillonite adsorbents. Part II: the effects of the type of raw clays and modification conditions on the adsorption performance. Chemosphere. 2003;53:53–62. https://doi.org/10.1016/S0045-6535(03)00449-1.
36. Sharma S, Sarasan G. Influence of acid activation on natural calcium montmorillonite clay. IOSR-JAC. 2017;10(6):71–7.
37. Ahmed A, Chaker Y, Belarbi EH, Abbas O, Chotard JN, Abassi HB, Nguyen Van Nhien A, El Hadri M, Bresson S. XRD and ATR/FTIR investigations of various montmorillonite clays modified by monocationic and dicationic imidazolium ionic liquids. J Mol Struct. 2018;1173:653–64. https://doi.org/10.1016/j.molstruc.2018.07.039.
38. Ates E, Uyanık N, Kızılcan N. Preparation of urea formaldehyde resin/layered silicate nanocomposites. Pigment Resin Technol. 2013;42:283–7. https://doi.org/10.1108/PRT-07-2012-0043.
39. Kašić V, Mihajlović S, Životić D, Simić V, Stojanović J, Sekulić Ž, Kragović M. Karakterizacija zeolitskog tufa iz ležišta „Igroš-Vidojevići“ sa geološkog i tehnološkog aspekta. Hem Ind. 2018;72:29–37. https://doi.org/10.2298/HEMIND170428015K.
40. Zivica V, Palou MT. Physico-chemical characterization of thermally treated bentonite. Compos Part B Eng. 2015;68:436–45. https://doi.org/10.1016/j.compositesb.2014.07.019.
41. Tiwari RR, Khilar KC, Natarajan U. Synthesis and characterization of novel organo-montmorillonites. Appl Clay Sci. 2008;38:203–8. https://doi.org/10.1016/j.clay.2007.05.008.
42. Qiu J, Jiang S, Wang Y, Chen G, Liu D, Liu X, Wang G, Wu P, Lyu X. Crystal chemistry characteristics and dispersion performance of Ca-montmorillonite with different layer charge density. Mater Res Express. 2020. https://doi.org/10.1088/2053-1591/aba803.
43. Ebewele OR, Myers EG, River HB, Koutsky AJ. Polyamine-modified urea-formaldehyde resins. I. Synthesis, structure, and properties. J Appl Polym Sci. 1991;42(11):2997–3012. https://doi.org/10.1002/app.1991.070421118.
44. Park DB, Jeong HN. Hydrolitic stability and crystallinity of cured urea-formaldehyde resin adhesives with different formaldehyde/urea mole ratios. Int J Adhes Adhes. 2011;31:524–9. https://doi.org/10.1016/j.ijadhadh.2011.05.001.
45. Chow C, Steiner RP. Catalytic, exothermic reactions of urea-formaldehyde resin. Holzforschung. 1975;29(1):4–10. https://doi.org/10.1515/hfsg.1975.29.1.4.
46. Liu M, Thirumalai RVKG, Wu Y, Wan H. Characterization of the crystalline regions of cured urea formaldehyde resin. RSC Adv. 2017;7:49536–41. https://doi.org/10.1039/C7RA08082D.
47. Marques IJ, Vaz PD, Fernandes AC, Nunes CD. Advantageous delivery of nifedipine from inorganic materials showing increased solubility and biocompatibility. Microporous Mesoporous Mater. 2014;183:192–200. https://doi.org/10.1016/j.micromeso.2013.09.021.
48. Zhou Y, Yang M, Zheng Y, Tong D, Zhou C, Yu W. Effect of a novel environmentally friendly additive of polyaspartic acid on the properties of urea formaldehyde resins/montmorillonite. Appl Polym Sci. 2019;136:48038. https://doi.org/10.1002/app.48038.
49. Wibowo ES, Lubis MAR, Park BD. In-situ modification of low molar ratio urea–formaldehyde resins with cellulose nanofibrils for plywood. J Adhes Sci Technol. 2021. https://doi.org/10.1080/01694243.2021.1890370.
50. Zhao Y, Wang K, Zhu F, Xue P, Jia M. Properties of poly(vinyl chloride)/wood flour/montmorillonite composites: effects of coupling agents and layered silicate. Polym Degrad Stabil. 2006;91:2874–83. https://doi.org/10.1016/j.polymdegradstab.2006.09.001.
51. Wibowo ES, Park BD. Enhancing adhesion of thermosetting urea-formaldehyde resins by preventing the formation of H-bonds with multi-reactive melamine. J Adhes. 2020. https://doi.org/10.1080/00218464.2020.1830069.
52. Wibowo ES, Lubis MAR, Park BD, Kim JS, Causin V. Converting crystalline thermosetting urea–formaldehyde resins to amorphous polymer using modified nanoclay. J Ind Eng Chem. 2020;87:78–89. https://doi.org/10.1016/j.jiec.2020.03.014.
53. Giroto AS, Guimarães GGF, Ribeiro CA. Novel, simple route to produce urea:urea–formaldehyde composites for controlled release of fertilizers. J Polym Environ. 2018;26:2448–58. https://doi.org/10.1007/s10924-017-1141-z.
54. Leszczynska A, Njuguna J, Pielichowski K, Banerjee JR. Review polymer/montmorillonite nanocomposites with improved thermal properties Part I. Factors influencing thermal stability and mechanisms of thermal stability improvement. Thermochim Acta. 2007;453:75–96. https://doi.org/10.1016/j.tca.2006.11.002.
55. Leszczynska A, Pielichowski K. Application of thermal analysis methods for characterization of polymer/montmorillonite nanocomposites. J Therm Anal Calorim. 2008;93:677–87. https://doi.org/10.1007/s10973-008-9128-6.
56. Ge J, Hou H, Li Q, Graham MJ, Greiner A, Reneker DH, Harris FW, Cheng SZD. Assembly of well-aligned multiwalled carbon nanotubes in confined polyacrylonitrile environments: electrospun composite nanofiber sheets. J Am Chem Soc. 2004;126:15754–61. https://doi.org/10.1021/ja048648p.
57. Chrissafis K, Paraskevopoulos KM, Papageorgiou G, Bikiaris D. Thermal and dynamic mechanical behavior of bionanocomposites: fumed silica nanoparticles dispersed in poly(vinyl pyrrolidone), chitosan, and poly(vinyl alcohol). J Appl Polym Sci. 2008;105:1739–49. https://doi.org/10.1002/app.28818.

58. Chrissafis K, Pavlidou E, Paraskevopoulos KM, Beslikas T, Nianias N, Bikiaris D. Enhancing mechanical and thermal properties of PLLA ligaments with fumed silica nanoparticles and montmorillonite. J Therm Anal Calorim. 2011;105:313–23. https://doi.org/10.1007/s10973-010-1168-z.
59. Siimer K, Kaljuvee T, Christjanson P, Pehk T. Changes in curing behaviour of aminoresins during storage. J Therm Anal Calorim. 2005;80:123–30. https://doi.org/10.1007/s10973-005-0623-8.
60. Siimer K, Kaljuvee T, Christjanson P. Thermal behaviour of urea-formaldehyde resins during curing. J Therm Anal Calorim. 2003;72:607–17. https://doi.org/10.1023/A:1024590019244.
61. Samaržija-Jovanović S, Jovanović V, Konstantinović S, Marković G, Marinović-Cincović M. Thermal behavior of modified urea-formaldehyde resins. J Therm Anal Calorim. 2011;104:1159–66. https://doi.org/10.1007/s10973-010-1143-8.
62. Roumeli E, Papadopoulou E, Pavlidou E, Vourlias G, Bikiaris D, Paraskevopoulus KM, Chrissafis K. Synthesis, characterization and thermal analysis of urea–formaldehyde/nanoSiO_2 resins. Thermochim Acta. 2012;527:33–9. https://doi.org/10.1016/j.tca.2011.10.007.
63. Moya R, Rodríguez-Zúñiga A, Vega-Baudrit J, Álvarez V. Effects of adding nano-clay(montmorillonite) on performance of polyvinylacetate (PVAc) and urea-formaldehyde (UF) adhesives in Carapa guianensis, a tropical species. Int J Adhes Adhes. 2015;59:62–70. https://doi.org/10.1016/j.ijadhadh.2015.02.004.